

APR 30 1956

CONFIDENTIAL

Copy
RM SL56D02

CLASSIFICATION CANCELLED

NACA

RESEARCH MEMORANDUM

for the

Bureau of Aeronautics, Department of the Navy

SOME FLIGHT DATA FOR THE CHANCE VOUGHT REGULUS II MISSILE

TED NO. NACA AD 398

By Andrew R. Wineman

Langley Aeronautical Laboratory
Langley Field, Va.

CLASSIFICATION CHANGE

To *Unclassified*

By authority of *NASA Memo dtd 5-2-73*

Changed by *M. Ruder*

Date *6-11-73*

CLASSIFIED DOCUMENT

This document contains classified information affecting the National Defense of the United States within the meaning of the Espionage Act, USC 18:793 and 794. Its transmission or the revelation of its contents in any manner to an unauthorized person is prohibited by law.

NATIONAL ADVISORY COMMITTEE
FOR AERONAUTICS

WASHINGTON

APR 23 1956

CONFIDENTIAL

FILE COPY

To be returned to
the files of the National
Advisory Committee
for Aeronautics
Washington, D. C.

20

DECLASSIFIED

NATIONAL ADVISORY COMMITTEE FOR AERONAUTICS

RESEARCH MEMORANDUM

for the

Bureau of Aeronautics, Department of the Navy

SOME FLIGHT DATA FOR THE CHANCE VOUGHT REGULUS II MISSILE

TED NO. NACA AD 398

By Andrew R. Wineman

SUMMARY

A 0.12-scale longitudinal stability model of the Chance Vought Regulus II missile has been tested by utilizing the free-flight, rocket-powered-model technique. Lift, static stability, dynamic stability, trim, duct information, and drag have been determined through a Mach number range of 0.8 to 2.1. Estimates have been made for the effect of flexibility on lift and static stability. In general, the data are in good agreement with the data from tests of an 0.065-scale model of the same configuration made at the 4- by 4-foot supersonic pressure tunnel, and with the zero-lift, 0.12-scale rocket-powered drag models. Although the performance of the oblique-shock scoop-type inlet appeared satisfactory, the resulting external flow seemed to influence trim, static stability, and, possibly, lift and drag. Large negative pitching moment at zero lift was experienced at supersonic speeds.

INTRODUCTION

At the request of the Bureau of Aeronautics, Department of the Navy, the external aerodynamics and duct performance of the Chance Vought Regulus II (XRSSM-N-9) missile were investigated by the National Advisory Committee for Aeronautics.

The Regulus II is a turbojet-powered, surface-to-surface missile which can be launched from ship or submarine at medium range targets and cruise at speeds near $M = 2.0$. The missile has no horizontal tail and incorporates a high-fineness-ratio nose, thin, swept wings of low aspect ratio, a highly swept vertical tail, and a scoop inlet with an oblique shock diffuser.

DECLASSIFIED

NACA RM SL56D02

Longitudinal and lateral static stability and control characteristics have been determined from a 0.065-scale model at Mach numbers of 1.41, 1.61, and 2.01 in the Langley 4- by 4-foot supersonic pressure tunnel and are reported in references 1 and 2. Zero-lift drag of the missile was obtained for a Mach number range of 0.8 to 2.2 from two 0.12-scale rocket-boosted flight models and is presented in reference 3. As part of an overall program, the longitudinal stability, drag, and limited duct performance are presented in this paper for a Mach number range of 0.8 to 2.1. A 0.12-scale open-duct rocket-boosted flight model was used to obtain these data from tests conducted at the Langley Pilotless Aircraft Research Station at Wallops Island, Va.

SYMBOLS

Symbols and coefficients used in this paper are listed below. Wherever possible the letter symbols recommended by the American Standard Association in the publication "Letter Symbols for Aeronautical Sciences," ASA Y10.7-1954, were employed.

A	cross-sectional area, sq ft
b	span, ft
c	chord of airfoil, ft
\bar{c}	mean geometric chord, ft
D	drag, lb
I_y	mass moment of inertia in pitch, slug-ft ²
L	lift, lb
l	length from leading edge of \bar{c} , positive aft, ft
M	Mach number
M'	pitching moment, ft-lb
P	period of pitch oscillation, sec
p	pressure; free-stream static pressure when used without subscript, lb/sq ft
q	dynamic pressure, $\frac{\gamma}{2} p M^2$, lb/sq ft

DECLASSIFIED

R	Reynolds number
S	total wing area, sq ft
$t_{1/2}$	time required for model to damp to one-half amplitude, sec
V	velocity, ft/sec
w/w_0	ratio of mass flow of air through the duct to mass flow of air through a free-stream tube of area equal to the inlet capture area, A_1
y	coordinate along Y-axis
α	angle of attack, deg
β	angle of sideslip, deg
γ	ratio of specific heats of air
$\dot{\gamma}$	rate of change of flight-path angle, radians/sec
θ/L	projected angle between chord and root chord of a twisted wing for a unit lift load, deg/lb
C_D	drag coefficient, D/qS
C_L	lift coefficient, L/qS
C_m	pitching-moment coefficient, $M'/qS\bar{c}$
C_{m_0}	pitching-moment coefficient at zero lift

$$C_{L_\alpha} = \frac{\partial C_L}{\partial \alpha}, \text{ per deg}$$

$$C_{m_\alpha} = \frac{\partial C_m}{\partial \alpha}, \text{ per deg}$$

$$C_{m_q} = \frac{\partial C_m}{\partial \left(\frac{q\bar{c}}{2V} \right)}, \text{ per radian}$$

$$C_{m_{\dot{\alpha}}} = \frac{\partial C_m}{\partial \left(\frac{\dot{\alpha}\bar{c}}{2V} \right)}, \text{ per radian}$$

Subscripts:

ac	aerodynamic center
b	base
cg	center of gravity
d	duct
e	exit
i	inlet or internal
max	maximum
min	minimum
sl	standard sea-level condition
t	total
trim	trim conditions, $C_m = 0$

DESCRIPTION OF THE MODEL

A three-view sketch, shown as figure 1, illustrates pertinent characteristics of the 0.12-scale stability model of the Regulus II; photographs of the model are shown as figure 2. The configuration had monoplanar wings, a vertical tail, and a ventral fin, all of which were sweptback, thin, and of low aspect ratio. The fuselage was essentially a body of revolution with a nose fineness ratio of $4\frac{1}{2}$ and a moderately boattailed afterbody. An oblique-shock scoop-type inlet, with corresponding duct and boundary-layer bleed, was faired under the fuselage. Body nose contours, wing airfoil contours, and duct area distributions are the same as those shown in tables I and II of reference 3.

The wings were constructed from steel, the fins from aluminum alloy, and the fuselage was composite aluminum and mahogany with a fiber glass duct. The ventral fin, of the same plan form and section as the vertical tail, was employed in order to insure sufficient directional stability to eliminate cross-coupling motions between pitch and yaw. Seven pulse rockets, with a thrust impulse of 20 pound-seconds each, were fitted in the fuselage to disturb the model in pitch. With the exception of the ventral fin, pulse rocket holes, α - β indicator, and total-pressure

DECLASSIFIED

pickup, the external lines of the model were geometrically similar to the contours of the full-scale missile. The area of the base annulus of the model was proportionally larger than the missile to insure sonic velocities at the duct exit. It was assumed that these modifications did not affect the longitudinal stability.

Because of the flexibility of a joint in the fuselage just forward of the boundary-layer bleed (station 38 in fig. 1) the nose section of the model was statically loaded to determine its deflection characteristics. The maximum deflection for the design loads expected at $M = 2.0$ was less than $1/2^\circ$, but it was impossible to determine accurately the deflection of the nose in flight, since joint flexibility was a function of the friction between surfaces.

The model weighed 115 pounds and the center of gravity was located at 45.2 percent \bar{c} ahead of the mean geometric chord. The moment of inertia in pitch was 11.15 slug-ft² and the inclination of the principal axis was zero.

INSTRUMENTATION

A standard NACA telemeter, with the appropriate pickups, was installed in the model to provide continuous measurements of the following quantities throughout the flight test: angle of attack, angle of sideslip, normal acceleration, transverse acceleration, longitudinal acceleration, pitching acceleration, free-stream stagnation pressure, base pressure, duct static pressure, and differential pressure between duct total and static pressures.

The α - β indicator, shown in figures 1 and 2 and described in reference 4, was located on a sting approximately 1 foot ahead of the model; the free-stream total-pressure pickup was on top of the model near the center of gravity. In order to insure minimum errors caused by angular velocities and accelerations, all accelerometers were mounted as close to the center of gravity as possible. A slotted, integrating, total-pressure rake and manifold static-pressure orifices were located in the constant-area section of the duct at station 66, which was about 3 diameters forward of the exit minimum. Base pressure was measured from four manifold holes equally spaced around the annular base.

Free-stream static pressure and temperature were obtained at various altitudes from a rawinsonde balloon launched just prior to the flight model. Telemetered data of the model were correlated with the rawinsonde data by a continuous record of flight altitude obtained from SCR 584 tracking radar. Mach number was calculated from static pressure and

model stagnation pressure; this Mach number was checked with Mach number obtained from speed of sound and velocity measured by a CW Doppler velocimeter.

TESTS AND ANALYSIS

Tests

The model was launched from a mobile zero-length launcher at an elevation angle of 60° . It was boosted to supersonic speeds in 3 seconds by two solid-propellant Deacon rocket motors of 6,000 pounds thrust each. The model separated from the booster just prior to burnout by virtue of its lower drag-to-weight ratio and coasted to higher altitudes at decreasing flight speeds. The data were obtained during this decelerating portion of the flight at the test Reynolds number shown in figure 3(a) and at the flight static pressure shown by the ratio in figure 3(b). Lightly damped transients, obtained by disturbing the model from trim conditions with pulse rockets ignited at predetermined intervals, permitted the evaluation of static and dynamic properties of the model through the Mach number range.

The right wing of the model was loaded statically at five consecutive spanwise points along both the quarter- and half-chord lines; the vertical displacements of the leading and trailing edges of the wing were measured with dial gages located at the same spanwise stations. These were the only structural measurements used to calculate the aeroelastic properties of the wing, since the flexibility of a sweptback wing is controlled chiefly by twist due to bending θ/L . Loads used in the static test were within the design limits of the model and no structural damage to the wing or fuselage was noted.

Analysis

Aeroelasticity.— The aeroelastic properties of the wing for the test Mach number range were determined by the method outlined in reference 5 using measured structural influence coefficients (see figs. 4(a) and 4(b)) and from theoretical span-load distributions of references 6 and 7. A solution employing two spanwise strips and the relieving inertia terms was used; this solution was checked by a reiterating method which employed five spanwise strips and inertia terms. The ratio of rigid CL_α to elastic CL_α of the model is shown as figure 4(c); the corresponding forward shift in aerodynamic-center location is shown in figure 4(d).

Reduction of data.- The short-period oscillations in pitch resulting from pulse rocket disturbances were analyzed by methods shown in reference 8 to determine longitudinal static and dynamic stability, trim, and drag characteristics of the model. The total pitching moment, corrected for damping, was also determined directly from measured angular acceleration in pitch \ddot{q} by the following relation:

$$C_m = \frac{I_y \ddot{q}}{q S \bar{c}} - \left[(C_{m_q} + C_{m_{\dot{\alpha}}}) \left(\frac{\bar{c}}{2V} \right) \right] q + C_{m_{\ddot{\alpha}}} \left(\frac{\bar{c}}{2V} \right) \ddot{\gamma} \quad (1)$$

The last term $C_{m_{\ddot{\alpha}}} \left(\frac{\bar{c}}{2V} \right) \ddot{\gamma}$, which was negligible, was eliminated from the calculation; $(C_{m_q} + C_{m_{\dot{\alpha}}})$ was obtained from the logarithmic decrement of the damped pitch oscillations; and the pitching velocity q was obtained indirectly from the measured angle of attack and normal acceleration.

Besides stability data, limited information on the scoop-type duct was obtained from the two duct pressure measurements. Total-pressure recovery of the duct was determined directly from measured duct static pressure and the difference between duct static and duct integrated total pressure. The mass-flow ratio was then calculated from the following relation:

$$\frac{w}{w_0} = \frac{p_d A_d M_d}{p A_1 M} \left[\frac{1 + \left(\frac{\gamma - 1}{2} \right) M_d^2}{1 + \left(\frac{\gamma - 1}{2} \right) M^2} \right]^{1/2} \quad (2)$$

At free-stream Mach numbers less than $M = 1.1$, M_d was obtained from the ratio of static to total pressure measured in the duct, and A_d was the cross-sectional area of the duct at the measuring station. The Mach number calculated from the duct pressures was about 0.5, and, when the errors involved in the pressure measurements are considered, M_d would cause large errors in mass flow. More accurate measurements of w/w_0 were obtained when a normal shock was assumed at the section of minimum area near the duct exit ($M_d = 1.0$); the static pressure at this station was determined by using adiabatic channel relations with a 1-percent loss in total pressure from the measuring station. This method was used for free-stream Mach numbers greater than $M = 1.1$ when it was evident that the duct was choked.

When the mass flow and exit pressure of the duct were known, it was possible to obtain the internal drag of the model by determining the momentum loss between the entrance and exit of the duct near zero angle

of attack. The internal drag coefficient was obtained from the following relation:

$$C_{D,i} = \frac{2A_e}{S} \left[\frac{w}{w_o} \left(\frac{A_i}{A_e} \right) - \frac{P_e}{P} \left(\frac{M_e}{M} \right)^2 - \left(\frac{P_e - P}{\gamma P M^2} \right) \right] \quad (3)$$

Again, as in the mass-flow equation, the static pressure at the exit was obtained from pressure measurements in the duct and from standard flow tables. This pressure was only valid when the exit of the duct was choked; however, when the flow at the exit became subsonic, base pressure was used in lieu of the calculated exit pressure in the above equation. Base-drag coefficient was also determined by pressure measurements from the manifold orifices at the base annulus. Base- and internal-drag coefficients $C_{D,b}$ and $C_{D,i}$ were subtracted from the total minimum-drag coefficient as determined from the lift-drag polars to obtain external minimum drag. No attempt was made to estimate the additive drag caused by scoop spillage although it is quite apparent that it exists. Minimum external drag coefficient includes this additive drag.

In the lift-drag relations, it was assumed that the polars of C_D and C_L were parabolic; that is, dC_D/dC_L^2 was constant with C_L . It was then possible to calculate $(L/D)_{\max}$ and the lift at which it occurred by the following relations:

$$C_L'' = \sqrt{(C_L')^2 + \frac{C_{D_{\min}}}{dC_D/dC_L^2}} - C_L' \quad (4)$$

and

$$(L/D)_{\max} = \frac{1}{2 \left(\frac{dC_D}{dC_L^2} \right) C_L''} \quad (5)$$

where C_L' is lift coefficient at $C_{D_{\min}}$, and C_L'' is the lift coefficient at $(L/D)_{\max}$. The absolute magnitude of $(L/D)_{\max}$ is only as accurate as the measured variables dC_D/dC_L^2 , $C_{D_{\min}}$, and C_L' ; and dC_D/dC_L^2 was in most cases obtained from oscillations in the negative lift range. However, these values indicate the trend of $(L/D)_{\max}$ with Mach number.

DECLASSIFIED

Accuracy

The accuracy of a set of data is often difficult to determine since it involves not only an estimation of the precision of the measured quantities but an estimation of the systematic and accidental errors encountered in reducing the data to final form. The reliability of data is often substantiated by comparison of results obtained by different testing techniques, or by the repeatability of results using the same technique. Experience has shown that, when such comparisons can be made, the order of magnitude of the accuracy is indicated by the deviations of the results. However, a theoretical accuracy can be calculated by several methods, such as mean square error, probable error, or average error. The probable error of the final data of this analysis was calculated; the method is outlined in the appendix and the results are shown in tables I and II.

RESULTS AND DISCUSSION

As mentioned previously, data were obtained from the analysis of oscillatory motions of the flight model, with zero elevon deflection, resulting from pulse rocket disturbances in pitch. As a general rule, these data are determined for a smaller range of coefficients (lift, drag, and moment) at the higher test Mach numbers than at subsonic speeds. For instance, the dynamic pressure of this model was 18 times larger at $M = 2.1$ than at $M = 0.8$. An indication of the range of coefficients can be seen in figure 5 for three test Mach numbers. A majority of the data above $M = 1.2$ was at negative lift coefficients since the C_L range was small and the model trimmed negatively. With the ventral fin, the lateral stability of the model was sufficient at supersonic speeds to limit the angle of sideslip to less than $1/2^\circ$ and the roll rate to less than 1 radian per second. At transonic and subsonic speeds, maximum angle of sideslip was less than $1\frac{1}{2}^\circ$ and roll rate less than 2 radians per second.

Lift

The test range of lift coefficients and an indication of the linearity of C_L with angle of attack can be noted from figure 5(a). Although C_L varies nearly linearly with α , the average slope over the entire C_L range was from 2 to 4 percent higher than the values of C_{L_α} obtained at lift coefficients near zero. The lift-curve slopes obtained over the Mach number range for the flexible wing are shown in figure 6 with test points obtained from reference 1.

DECLASSIFIED

CONFIDENTIAL

NACA RM SL56D02

The estimated effect of wing flexibility on $C_{L\alpha}$, as shown by figure 4(c), indicates that the rigid lift-curve slope could be as much as 16 percent larger than the flexible $C_{L\alpha}$ at $M = 2.1$, but wing flexibility has little influence at subsonic Mach numbers. Although the accuracy of the estimated ratio of rigid to elastic lift is not known, the probable error of the flexible $C_{L\alpha}$ was calculated to be from 6 to 8 percent. Data from wind-tunnel tests of reference 1 fall within this accuracy band and agreement is considered good. The tunnel tests should be slightly higher for two reasons: the tunnel model was rigid for its test conditions and the mass flow through the duct of the tunnel model was slightly higher than the flight model at $M = 1.41$ and $M = 1.61$. Although the effect of mass flow on $C_{L\alpha}$ is not known, it is believed that decreasing mass flow would cause more spillage from the inlet over the wing root sections and decrease the slope of the lift curve.

Static Stability

The variation of period, $C_{m\alpha}$, and aerodynamic-center location with Mach number are shown in figure 7 for the center of gravity located at 45.2 percent of \bar{c} ahead of the leading edge of \bar{c} . It can be seen from figure 7(a) that, although the period is slightly erratic at transonic speeds, it is regular throughout the supersonic Mach number range. The variation of period in the transonic region is not entirely due to changes in static stability at zero lift, but is also influenced by nonlinearities of the static derivatives and the C_L range through which the model oscillated. For this reason the period obtained from transients that produced linear variations of C_m with C_L are shown separately from those obtained from nonlinear transients. Period from the linear transients was used to determine $C_{m\alpha}$, which is shown in figure 7(b). Between $M = 0.80$ and $M = 1.04$, $C_{m\alpha}$ and aerodynamic-center location (figs. 7(b) and (c)) are indicated by dashed lines because variations in the period permitted several possible fairings of period with Mach number. The location of the aerodynamic center was determined by two methods: by use of the ratio of $C_{m\alpha}$ to $C_{L\alpha}$ and by direct measurement of the static margin dC_m/dC_L at $C_m = 0$ from polars similar to samples shown in figure 5(b). These values are shown in figure 7(c) for the flexible wing. About the same accuracy was noted for both methods, varying from 4 to 6 percent of the mean geometric chord for the test Mach number range.

There is evidence that the strong detached shock in front of the inlet influenced static stability in the transonic region. As shown in




figure 7(a), between Mach numbers of 0.9 to 1.05 the period of the linear transients varied beyond the range of the calculated probable error of ± 0.005 . It is believed that the shock changed the pressure distribution over the inner wing panels and the fuselage afterbody sufficiently to cause at least part of these variations in period. In this Mach number range, however, the angle of attack was less than 1° and, in some cases, was as small as the angle of sideslip. Yet, as can be seen in figure 7(c), near $M = 1.1$ the aerodynamic-center location varied from 8 to 10 percent \bar{c} when determined from $C_m - C_L$ polars. This variation was immediately following a pulse rocket disturbance where α was considerably greater than the angle of sideslip. Similar variations in trim noted in the transonic region substantiate the belief that the shock from the inlet caused sufficient pressure changes over the wing and fuselage to influence the stability of the model.

At supersonic speeds the effect of flexibility tends to relieve the aerodynamic loads at the wing tips, causing the aerodynamic center to move forward. This forward shift, which was calculated and shown in figure 4(d), indicates that the rigid-wing aerodynamic center was about 7 percent \bar{c} aft of the flexible value shown in figure 7(c) for $M = 2.1$; smaller differences were experienced at lower Mach numbers. Rigid aerodynamic-center location compared with results from tests in the Langley 4- by 4-foot supersonic tunnel show the same rearward movement with increasing Mach numbers at supersonic speeds. The difference between the flight test and reference 1 may be attributed to different duct mass-flow ratios.

Within the accuracy of the data, the aerodynamic-center locations as obtained from the flight test by two independent measurements were in good agreement and were in reasonable agreement with reference 1. A total rearward shift of about 30 percent \bar{c} was noted for the flexible wing for a Mach number range of 0.8 to 2.1, and about 37 percent \bar{c} for the rigid wing. There are also indications that the static stability was not regular through the transonic region.

Dynamic Stability

The variation of total damping and the damping-in-pitch derivative with Mach number are shown in figure 8. The time required for the flight model to damp to half amplitude (fig. 8(a)) was obtained from the logarithmic decrement of the decaying oscillation resulting from pitch disturbances in flight. This logarithmic decrement was not constant with time or amplitude of oscillation, even after the effect of Mach number was taken into account. Although actual measurement of the logarithmic decrement was accurate enough, it is questionable if this represents the total damping of the model with the same degree of accuracy; for instance, the oscillations of rather small amplitudes may not be indicative of a

DECLASSIFIED

free motion in the pitch plane. In order to account for this, the values of $t_{1/2}$ shown in figure 8(a) were obtained from a faired average of the logarithmic decrements of the first few cycles of oscillation after the pitch disturbance. A corresponding band of probable error in $t_{1/2}$, as shown in table II, was assumed to include these unknown variations. An additional guide to the total damping is percent of critical damping, which was 6.1 at $M = 0.9$ and 4.5 at $M = 2.1$. However, these values cannot be applied directly to the full-scale missile, since the present model was not dynamically scaled.

The damping-in-pitch derivative ($C_{m\dot{q}} + C_{m\dot{\alpha}}$), shown in figure 8(b) was obtained from the difference between the total damping and the lift component. Because the quantity ($C_{m\dot{q}} + C_{m\dot{\alpha}}$) is the difference between two nearly equal quantities, the error of the derivative can become large, especially at lower Mach numbers, as shown in table II. In general, the damping-in-pitch derivative was small, around -10 per radian, but was about the same magnitude as experienced by other tailless configurations discussed in reference 10. There were no unusual changes with Mach number.

Trim

Trim characteristics of the model, shown in figure 9, all tend to be negative throughout the test Mach number range. Changes in trim were experienced through the transonic region, and relatively large negative values of trim were indicated for supersonic Mach numbers. Figure 9 also shows these data compared with results from reference 1. The pitching moment at zero lift from reference 1 is also shown in figure 9, without corrections for flight mass-flow ratios.

The nature of the trim of this configuration seems largely influenced by the underslung duct and the boundary-layer bleed. As mentioned in other sections, the fluctuations of the detached inlet shock were believed to have caused variations in trim between $M = 0.9$ and $M = 1.3$. As indicated in references 1 and 2, the mass flow of both the duct and boundary-layer bleed affect C_{m_0} .

Reasonable changes in mass flow, $w/w_0 = 0.9$ to $w/w_0 = 1.0$, can change C_{m_0} as much as 30 percent at $M = 2.1$, as shown by reference 1. When C_{m_0} of reference 1 was corrected for the mass flow of the flight model, the agreement of the data was good. Flight values of C_{m_0} were slightly larger, although within the probable error as shown in table II, except near the maximum Mach number. As mentioned in reference 2, it was believed that part of the large C_{m_0} at supersonic speeds may have been

DECLASSIFIED

caused by flexibility of the long nose; wind-tunnel tests were made at $M = 2.01$ for different nose deflections to determine this effect. Although it appears possible that nose bending contributed to the negative values of C_{m_0} , the influence of flexibility on the C_{m_0} of the flight model was considered small compared to total pitching moment at zero lift.

Because of the large negative C_{m_0} at supersonic speeds, large elevon deflections would be required to trim at positive lift coefficients. A positive shift in C_{m_0} due to the addition of fixed incidence, horizontal canard surfaces on the nose was reported in reference 2.

Duct

Operation of the inlet was satisfactory throughout the Mach number range of 0.8 to 2.2. The total-pressure recovery $\frac{P_{t,d}}{P_t}$ and the mass-flow ratio, w/w_0 , of the duct are shown for zero angle of attack in figure 10. As shown previously, some of the data in reference 1, which were compared with the flight data, were influenced by the mass flow of the duct; therefore w/w_0 for the test points of reference 1, are also shown in figure 10(b). These parameters also varied with angle of attack similar to the samples shown in figures 5(d) and 5(e).

The maximum measured variation of $\frac{P_{t,d}}{P_t}$ and w/w_0 due to angle of attack occurred at $M = 1.56$ and was about 10 percent for an α range of 8° . Only limited data on the duct could be obtained at positive angles of attack, since the model trimmed at negative angles of attack throughout the flight. At Mach numbers greater than 1.6, total-pressure recovery and mass flow decreased with increasing positive α , but for Mach numbers less than 1.6, increased for increasing positive α . For $\alpha = 0^\circ$ at the design Mach number of the inlet, $M = 2.0$, recovery was 0.77 and mass flow was 1.0.

The duct appeared stable for the ranges of Mach number and angle of attack tested. The duct started immediately upon separation from the booster at $M = 2.18$. Additional indication of duct stability was demonstrated near $M = 2.0$ as a pulse rocket discharged just forward of the inlet. Although this caused a sharp pressure jump ahead of the inlet, flow was stabilized in the duct within 0.02 second. However, random duct pressure variations of ± 1 pound per square inch were noted from $M = 1.5$ to $M = 2.18$. It is believed this turbulence was caused by interaction of the shock from the boundary-layer bleed and the shock from the inlet lip. As a larger portion of the inlet was covered by a normal shock, the random pressure variations in the duct discontinued.


Drag

The variation of minimum drag characteristics with Mach number is shown in figure 11. Base- and internal-drag coefficients are demonstrated in figure 11(a). The maximum contribution of $C_{D,b}$ to $C_{D_{min}}$ is about 8 percent of $C_{D_{min}}$. The variation of $C_{D,b}$ with angle of attack was always less than 1 percent of $C_{D_{min}}$. Internal-drag coefficient, as calculated from the total momentum loss in the duct, is a direct function of mass flow and attains a maximum at $M = 1.9$ of 12 percent of $C_{D_{min}}$. The contribution of $C_{D,i}$ and $C_{D,b}$ to $C_{D_{min}}$ nearly nullify each other at subsonic speeds, whereas at higher Mach numbers they are additive to the external minimum-drag coefficients.

The variation of $C_{D_{min}}$ with Mach number is shown in figure 11(b). External-drag coefficient is the total minimum-drag coefficient less $C_{D,i}$ and $C_{D,b}$ of figure 11(a). The external $C_{D_{min}}$ varied from 0.024 at subsonic speeds to a maximum of 0.045 at $M = 1.25$ and reduced to 0.034 at $M = 2.01$. These values of external $C_{D_{min}}$ were slightly larger than those indicated by data from tunnel tests of reference 1; however, good agreement was noted when the total $C_{D_{min}}$ was compared with the zero-lift data from the flight test of model 2, as reported in reference 3.

The importance of trim lift on total drag is shown by the lift-drag relations in figure 12. The drag due to lift dC_D/dC_L^2 was obtained mostly from data at negative lift coefficients, and, as shown in reference 1, is slightly higher than dC_D/dC_L^2 at positive lift. For the same range of C_L , results obtained in the 4- by 4-foot supersonic tunnel agreed favorably with the flight test. Little or no leading-edge suction was obtained since the test points are close to $1/C_{L_{\alpha}}$; full leading-edge suction is indicated by $\frac{1}{\pi(\text{aspect ratio})}$.

By measuring the value of dC_D/dC_L^2 , $C_{D_{min}}$, and C_L at $C_{D_{min}}$, it was possible to estimate the maximum lift-to-drag ratio and C_L at which it occurred for zero control deflection. Most oscillations in flight did not attain sufficient positive C_L to reach $(L/D)_{max}$; however, $(L/D)_{max}$ from the polars that did attain sufficient positive C_L to reach $(L/D)_{max}$ are shown in figure 12. Since the variation of C_D with C_L^2 was linear, it was possible to assume parabolic polars and calculate $(L/D)_{max}$ and the corresponding C_L . For supersonic speeds $(L/D)_{max}$ remained constant



DECLASSIFIED

at about 4.5 and would require a $C_L = 0.3$. From tunnel tests of this configuration an elevon deflection of 20° was needed to attain $C_L = 0.07$ at $M = 2.01$. This value is only about a fourth of the deflection required for $(L/D)_{\max}$ as shown in figure 12. This value of $(L/D)_{\max}$ is optimistic, since the drag due to the control deflection required for trim is not included. Less elevon deflection would be required to trim at $(L/D)_{\max}$ if C_{m_0} were made more positive.

CONCLUSIONS

The conclusions reached from the analysis of the free-flight test of a 0.12-scale longitudinal stability model of the Chance-Vought Regulus II missile can be summarized as follows:

1. The variation of lift with angle of attack is fairly linear for the test Mach number range, and it is estimated that the lift-curve slope C_{L_α} is subject to a maximum reduction of 16 percent at a Mach number of 2.1 due to wing flexibility. Agreement with the data obtained in the Langley 4- by 4- foot supersonic pressure tunnel is good.

2. The aerodynamic center shifted rearward 30 percent of the mean geometric chord for a Mach number increase of 0.8 to 2.1, with an estimated additional movement of 7 percent of the mean geometric chord for a rigid wing. There was evidence that the static stability was not regular at transonic speeds; a variation of 8 to 10 percent of mean geometric chord was noted in the static margin at a Mach number of 1.1. The aerodynamic-center location of the rigid wing demonstrated the same rearward trend at supersonic speeds as shown in NACA Research Memorandum SL55E31. It is believed that different mass flow in the duct caused a more rearward aerodynamic-center location in flight test than shown by tests in the Langley 4- by 4-foot supersonic pressure tunnel.

3. Total damping of the model was about 5 percent of critical. Damping-in-pitch derivative $(C_{m_q} + C_{m\dot{\alpha}})$ exhibited no unusual trends and remained nearly constant with Mach number. A value of $(C_{m_q} + C_{m\dot{\alpha}}) = -10$ per radian was noted, which is reasonable for tailless configurations.

4. Trim remained negative for the entire Mach number range; the trim was rather large at $M = 2.0$, but at transonic speeds it was reduced to near zero, although it exhibited slight variations with Mach number. It is believed that trim characteristics were influenced by changes in flow patterns at the inlet. The pitching moment at zero lift is considered

DECLASSIFIED

NACA RM SI56D02

to be too large negatively to permit trim near minimum drag coefficient or maximum lift-to-drag ratio without exceeding elevon deflections of 20° .

5. The duct was stable for all Mach numbers with slight turbulence in the Mach number range from 1.5 to 2.1 believed to have resulted from shock interference at the inlet. At design Mach number, $M = 2.0$, the inlet experienced total-pressure recovery of 0.77 and a mass-flow ratio of 1.0. At a Mach number of 1.6, a 10-percent variation of total-pressure recovery and mass flow was produced by an 8° change in angle of attack.

6. The minimum external-drag coefficient varied from 0.024 at subsonic speeds to a maximum of 0.045 at a Mach number of 1.25 and a value of 0.034 at a Mach number of 2.0. This variation was slightly larger than indicated by data obtained from the Langley 4- by 4-foot supersonic pressure tunnel but drag data from a previously tested zero-lift flight model was substantiated. The maximum lift-to-drag ratio $(L/D)_{\max}$ for zero control deflection, was constant with Mach number for supersonic speeds at a value not greater than 4.5.

Langley Aeronautical Laboratory,
National Advisory Committee for Aeronautics,
Langley Field, Va., April 4, 1956.

Andrew R. Wineman

Andrew R. Wineman
Aeronautical Research Scientist

Approved:

Joseph A. Shortal
Joseph A. Shortal
Chief of Pilotless Aircraft Research Division

mfh



APPENDIX

ACCURACY

The method used to estimate the accuracy of the data was obtained from the chapter entitled "The Precision of Measurements" in reference 9. In this analysis, probable error was used to indicate the accuracy of the results.

If a large number of direct measurements were made of a single quantity, and all deviations noted, the magnitude of the probable error r may be defined as such that half of the total number of deviations are greater than r and half are less than r . That is, the probability that the error of a single measurement will fall between $+r$ and $-r$ is one-half.

It was assumed that the flight measurements had a probable error of $\pm 1/2$ percent of the calibrated instrument range. Mach number was also assumed to be a direct measurement to facilitate calculations. This assumption was substantiated by the fact that Mach numbers closely agreed when calculated from two nearly independent sets of measurements: from model stagnation pressure in conjunction with rawinsonde static pressure, and from CW Doppler velocity in conjunction with rawinsonde speed of sound. The probable error in Mach number then was estimated from the assumed errors in rawinsonde static and model stagnation pressures. The assumed probable errors of the directly measured quantities are shown in table I.

From reference 9, the probable error of the indirect measurements, such as the final data, may be estimated by the following equation:

$$R = \sqrt{\left(\frac{\partial Q}{\partial q_1}\right)^2 r_1^2 + \left(\frac{\partial Q}{\partial q_2}\right)^2 r_2^2 + \left(\frac{\partial Q}{\partial q_3}\right)^2 r_3^2 + \dots + \left(\frac{\partial Q}{\partial q_n}\right)^2 r_n^2} \quad (A1)$$

where R is the probable error of the indirect quantity Q , and Q is a function of the direct measurements, $q_1, q_2, q_3, \dots, q_n$, each with a probable error of $r_1, r_2, r_3, \dots, r_n$. In order to apply equation (A1), the relation between the direct measurements and the final result must be established mathematically. For instance, the lift-curve slope was measured directly from a plot of C_L against α , but for error calculations it was first necessary to assume the equation of a line passing through at least two representative points from the measured data, then to express the slope of this line with respect to normal acceleration,

DECLASSIFIED

NACA RM SL56D02

longitudinal acceleration, angle of attack, Mach number, static pressure, model weight, and wing area. This facilitates the partial differentiation of $C_{L\alpha}$ with respect to the independent variables, as required for equation (A1). A similar technique was used for the final data and the estimated errors are shown in table II.

REFERENCES

1. Robinson, Ross B., Driver, Cornelius, and Spearman, M. Leroy: Static Longitudinal and Lateral Stability and Control Characteristics of an 0.065-Scale Model of the Chance Vought Regulus II Missile at Mach Numbers of 1.41, 1.61, and 2.01 - TED No. NACA AD 398. NACA RM SL55E31, Bur. Aero., 1955.
2. Robinson, Ross B., and Driver, Cornelius: Effects of Various Modifications on the Static Longitudinal Stability and Control Characteristics of a 0.065-Scale Model of the Chance Vought Regulus II Missile at a Mach Number of 2.01 - TED No. NACA AD 398. NACA RM SL55I15, Bur. Aero., 1955.
3. Church, James D.: Zero-Lift Drag of the Chance Vought Regulus II Missile at Mach Numbers Between 0.8 and 2.2 as Determined From the Flight Tests of Two 0.12-Scale Models - TED No. NACA AD 398. NACA RM SL54H02, Bur. Aero., 1954.
4. Ikard, Wallace L.: An Air-Flow-Direction Pickup Suitable for Telemetering Use on Pilotless Aircraft. NACA RM L53K16, 1954.
5. Vitale, A. James: Effects of Wing Elasticity on the Aerodynamic Characteristics of an Airplane Configuration Having 45° Sweptback Wings As Obtained From Free-Flight Rocket-Model Tests at Transonic Speeds. NACA RM L52L30, 1953.
6. DeYoung, John, and Harper, Charles W.: Theoretical Symmetric Span Loading at Subsonic Speeds for Wings Having Arbitrary Plan Form. NACA Rep. 921, 1948.
7. Martin, John C., and Jeffreys, Isabella: Span Load Distributions Resulting From Angle of Attack, Rolling, and Pitching for Tapered Sweptback Wings With Streamwise Tips - Supersonic Leading and Trailing Edges. NACA TN 2643, 1952.
8. Gillis, Clarence L., Peck, Robert F., and Vitale, A. James: Preliminary Results From a Free-Flight Investigation at Transonic and Supersonic Speeds of the Longitudinal Stability and Control Characteristics of an Airplane Configuration With a Thin Straight Wing of Aspect Ratio 3. NACA RM L9K25a, 1950.
9. Scarborough, James B.: Numerical Mathematical Analysis. The Johns Hopkins Press (Baltimore), 1950.
10. Gillis, Clarence L., and Chapman, Rowe, Jr.: Summary of Pitch-Damping Derivatives of Complete Airplane and Missile Configurations As Measured in Flight at Transonic and Supersonic Speeds. NACA RM L52K20, 1953.

CONFIDENTIAL

TABLE I

PROBABLE ERRORS ASSUMED IN DIRECT MEASUREMENTS

[All values for error and percent error are plus or minus. Instrumentation errors are assumed to be 10.5 percent of the calibration range. The symbol p_t' represents stagnation pressure as measured by pitot tube.]

(a) Geometry and Mass Characteristics

	W	I_y	\bar{x}	S	l_{cg}	A_1	A_e	A_p
Quantity	115	11.15	0.873	2.08	0.394	0.0464	0.0358	0.0127
Error	.5	.206	.0014	.002	.0104	.00003	.00003	.00003
Percent error	.4	1.8	.2	.1	2.6	.1	.1	.2

(b) Flight Measurements

	Mach number			Normal acceleration			Longitudinal acceleration			Pitching acceleration			Angle of attack		
Mach number	0.89	1.38	2.10	0.89	1.38	2.10	0.89	1.38	2.10	0.89	1.38	2.10	0.89	1.38	2.10
Quantity	.69	1.38	2.10	-4.52	5.87	-11.84	-.14	-1.01	-3.79	22.8	42.6	57.6	-8.88	-4.44	-2.39
Error	.036	.012	.006	.150	.150	.150	.030	.030	.030	.69	1.34	1.69	.050	.050	.050
Percent error	4.0	.9	.3	3.3	2.5	1.3	22.4	3.0	1.3	3.0	3.1	3.0	.6	1.1	1.7

	P			P_d			$(P_{t,d} - P_d)$			P_b			P_t'		
Mach number	0.89	1.38	2.10	0.89	1.38	2.10	0.89	1.38	2.10	0.89	1.38	2.10	0.89	1.38	2.10
Quantity	5.18	7.96	12.64	7.4	18.5	70.6	1.28	3.64	11.86	5.24	6.18	8.49	8.7	23.7	80.4
Error	.029	.029	.029	.42	.42	.42	.130	.130	.130	.050	.050	.050	.34	.34	.34
Percent error	5.6	.4	.2	5.6	2.3	.6	10.2	3.6	1.1	1.0	.8	.6	3.9	1.7	.5

TABLE II

PROBABLE ERRORS IN DATA

[All values for probable errors are plus or minus]

Quantity	Mach number		
	0.89	1.38	2.10
$C_{L\alpha}$	0.0049	0.0030	0.0026
P	.005	.002	.002
$C_{m\alpha}$.0025	.0018	.0011
$l_{ac}(C_{m\alpha}/C_{L\alpha})$	5.36	5.75	5.98
$l_{ac}(dC_m/dC_L)$	5.68	4.34	5.30
$t_{1/2}$.237	.072	.014
$C_{mq} + C_{m\dot{\alpha}}$	3.21	4.66	1.69
x_{trim}	.25	.25	.25
C_{Ltrim}	.0216	.0152	.0052
C_{m0}	.0155	.0149	.0039
$P_{t,d}/P_t$.063	.024	.004
w/w_0	.194	.018	.007
$C_{D,b}$.00048	.00018	.00007
$C_{D,i}$.0094	.0016	.00047
$C_{Dmin}(total)$.0048	.0039	.0014
dC_D/dC_L^2	.011	.134	.187

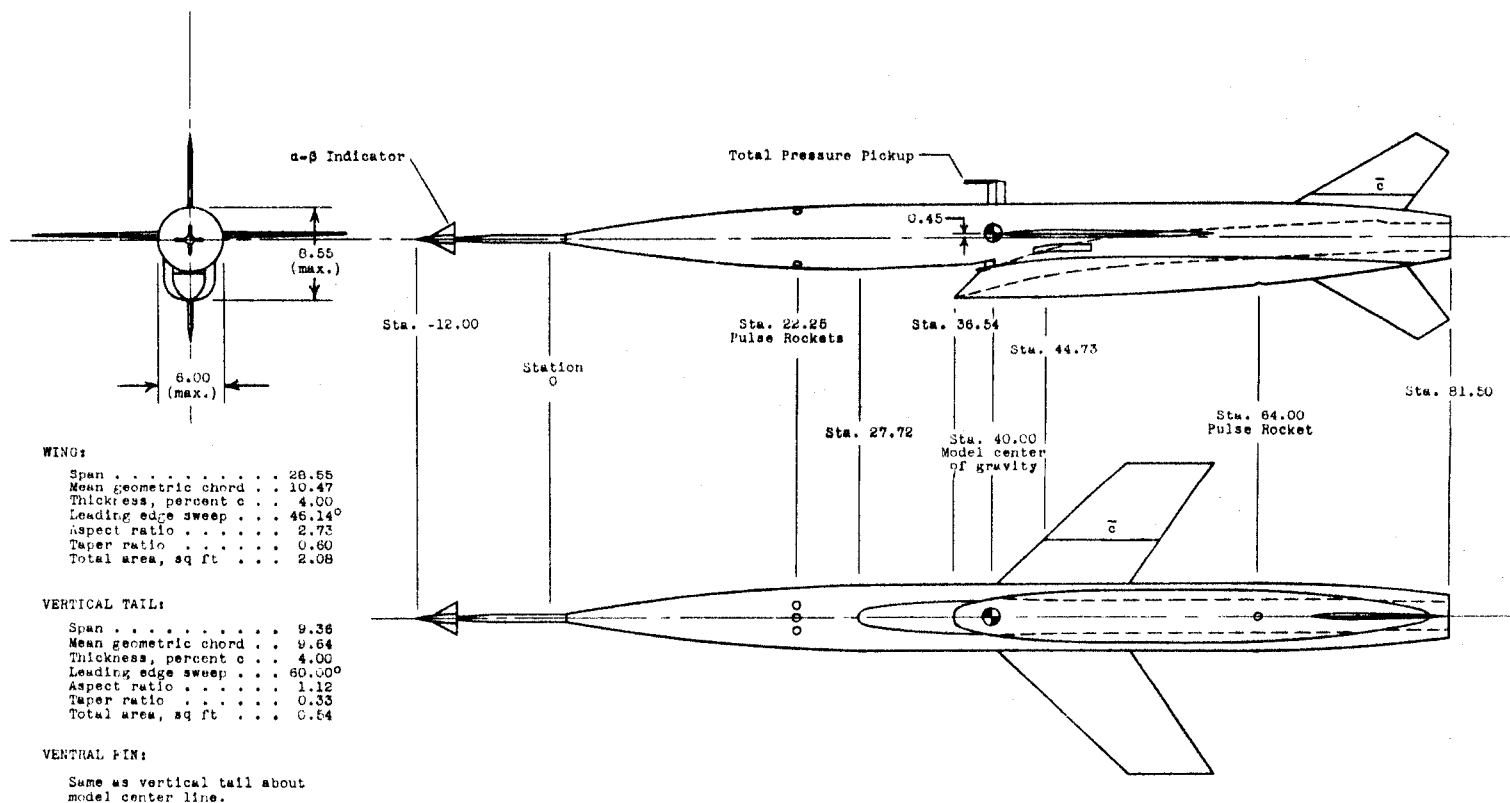
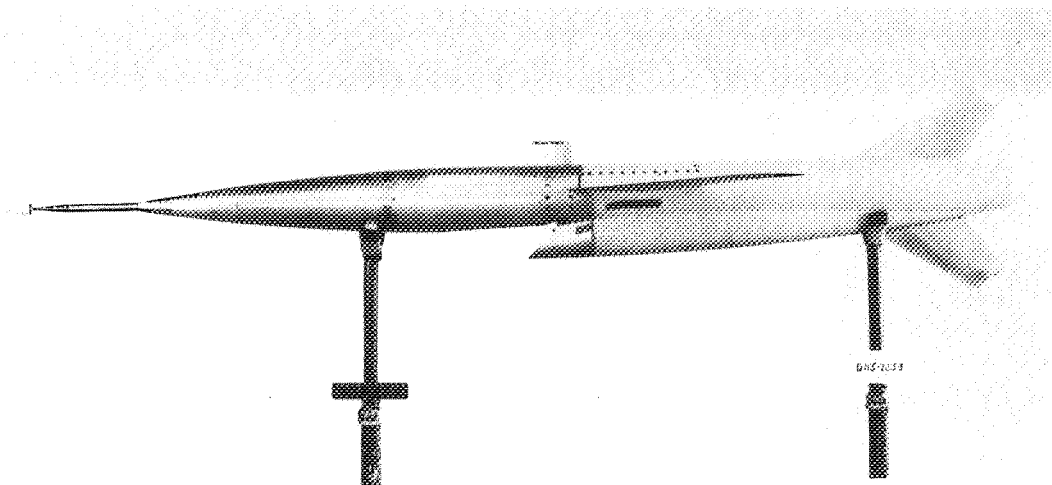
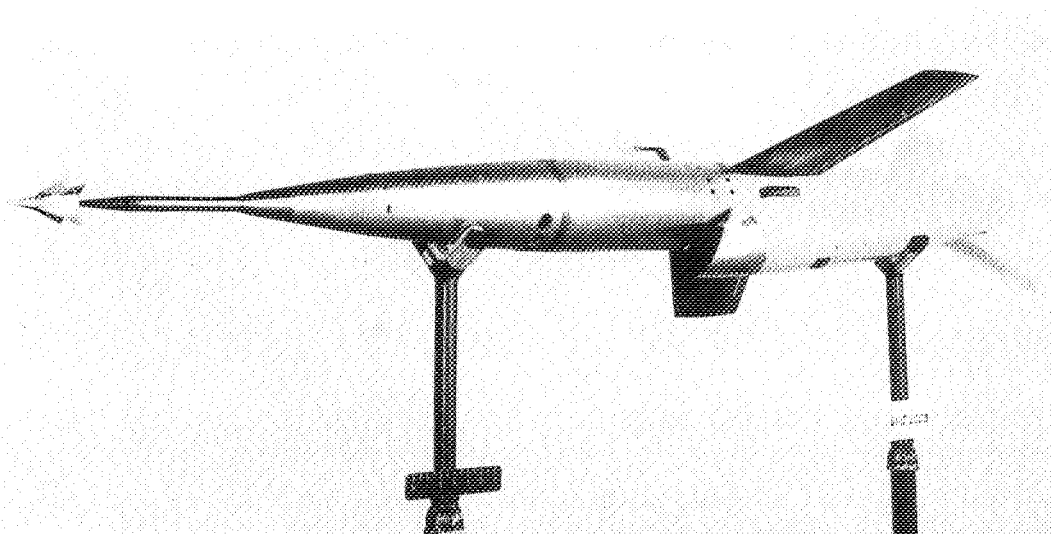


Figure 1.- General arrangement of 0.12-scale stability model. All dimensions are in inches.



(a) Side view.

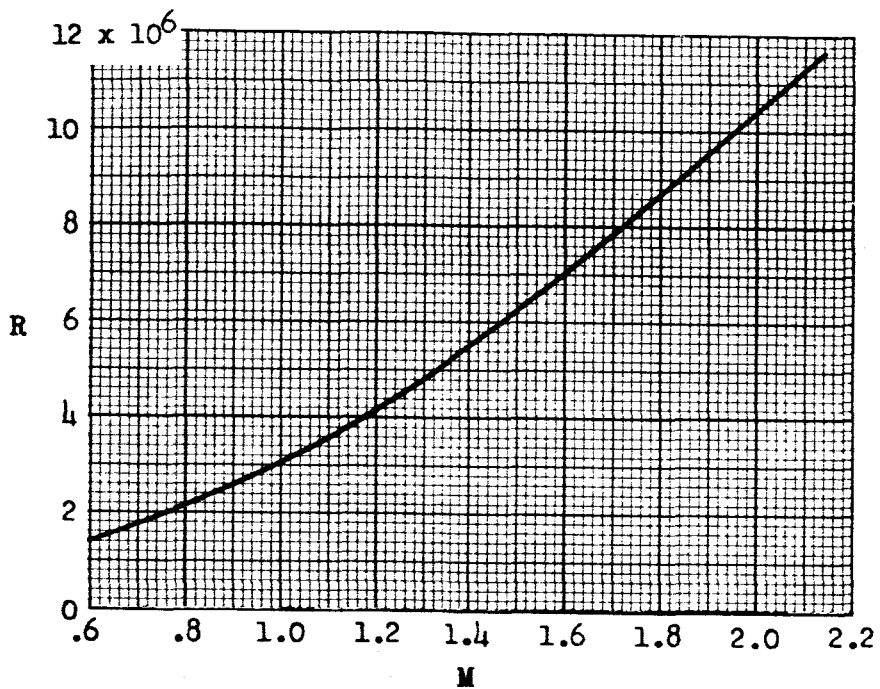
L-85682.1



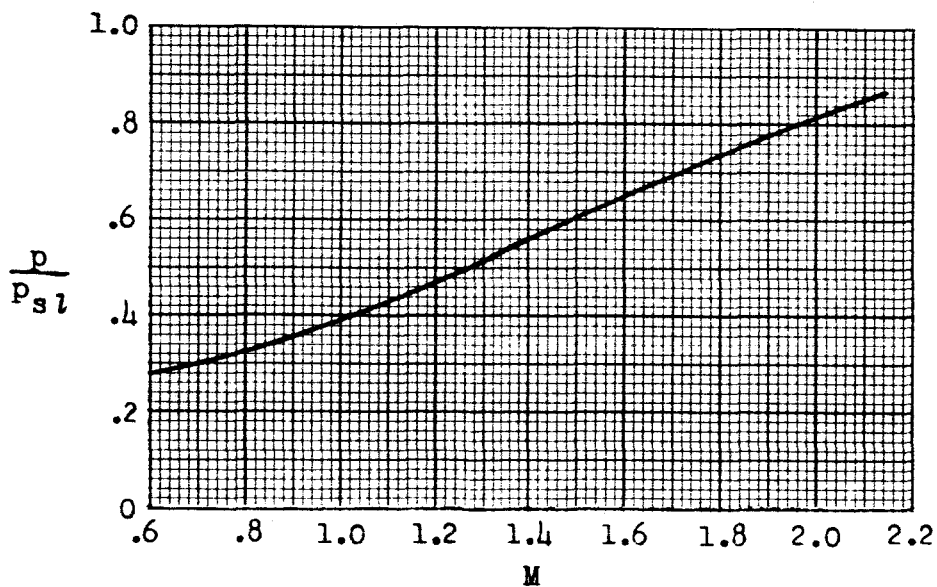
(b) Three-quarter front view.

L-85685.1

Figure 2.- Photographs of model.



(a) Reynolds number; based on \bar{c} .

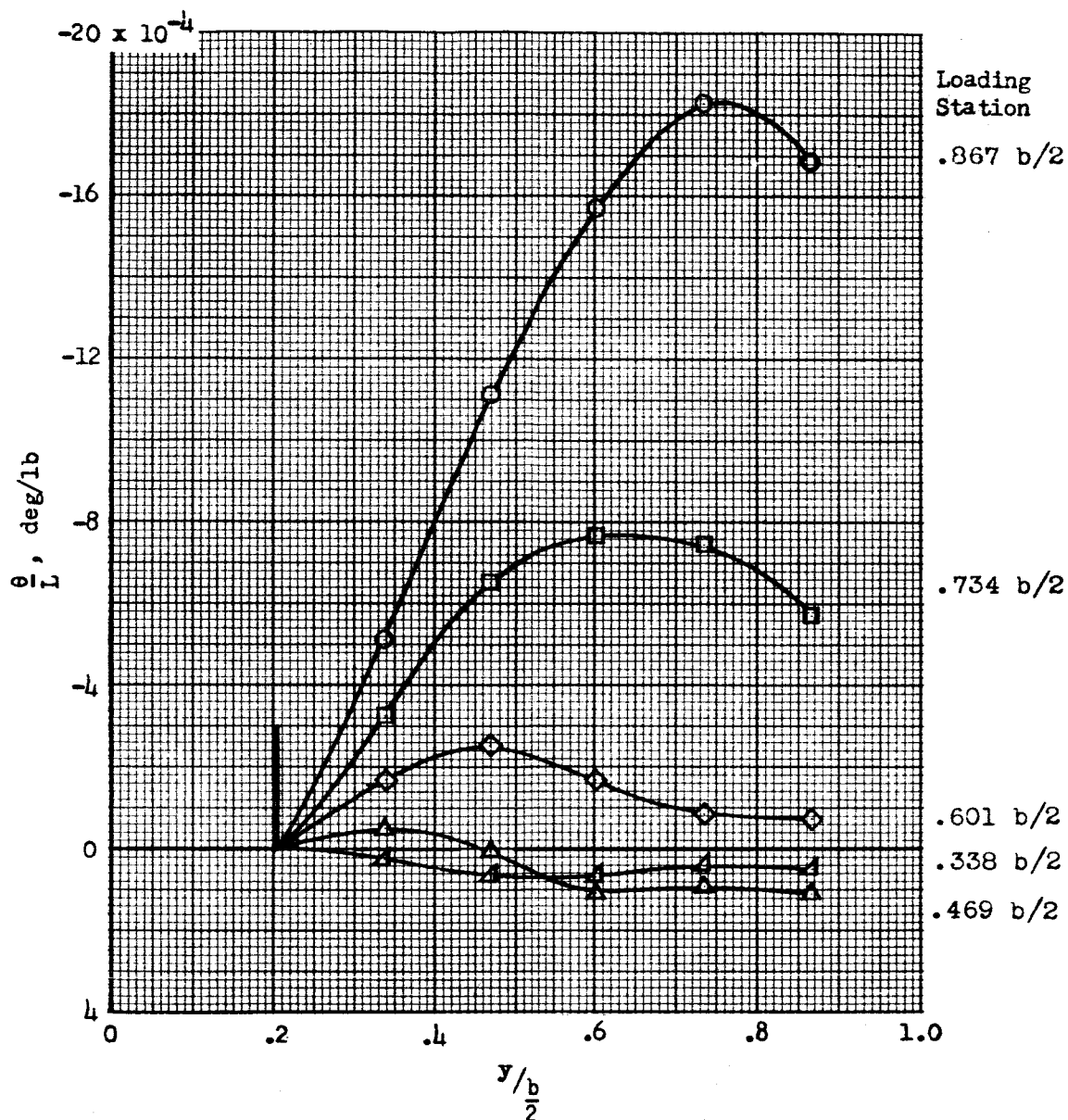


(b) Static pressure ratio.

Figure 3.- Flight test conditions.

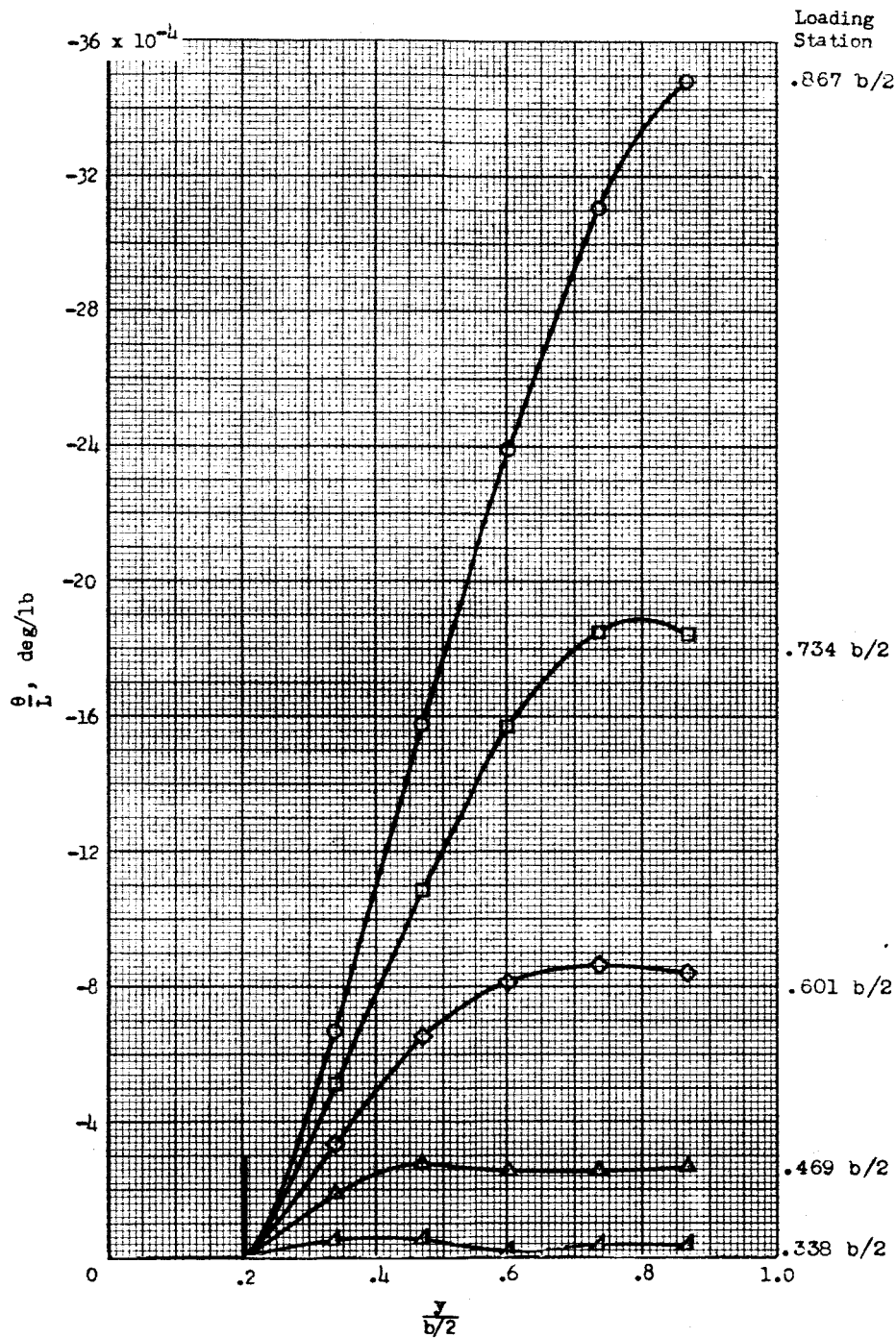
DECLASSIFIED

CONFIDENTIAL



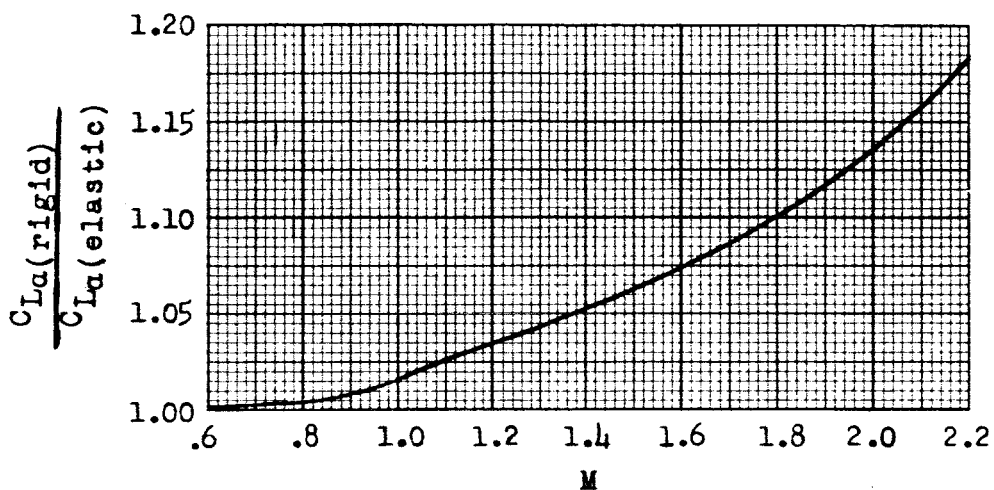
(a) Structural influence coefficients for 0.25c loading.

Figure 4.- Aeroelastic properties of wing.

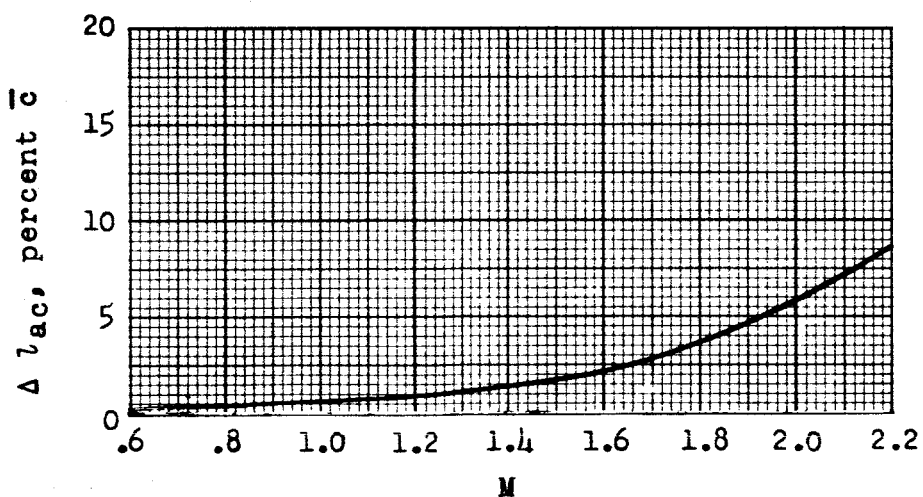


(b) Structural influence coefficients for 0.50c loading.

Figure 4.- Continued.

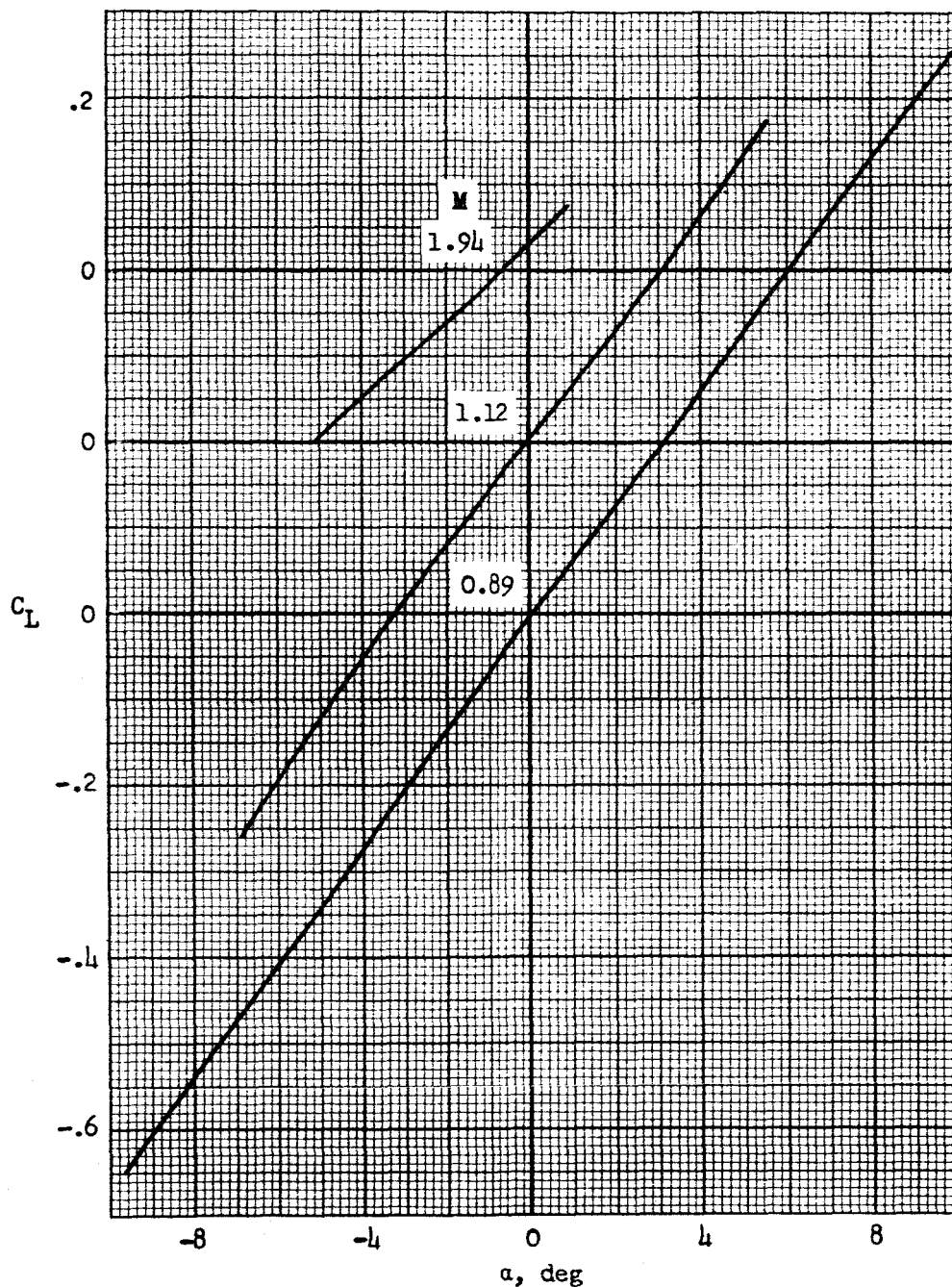


(c) Ratio of rigid lift to elastic lift.



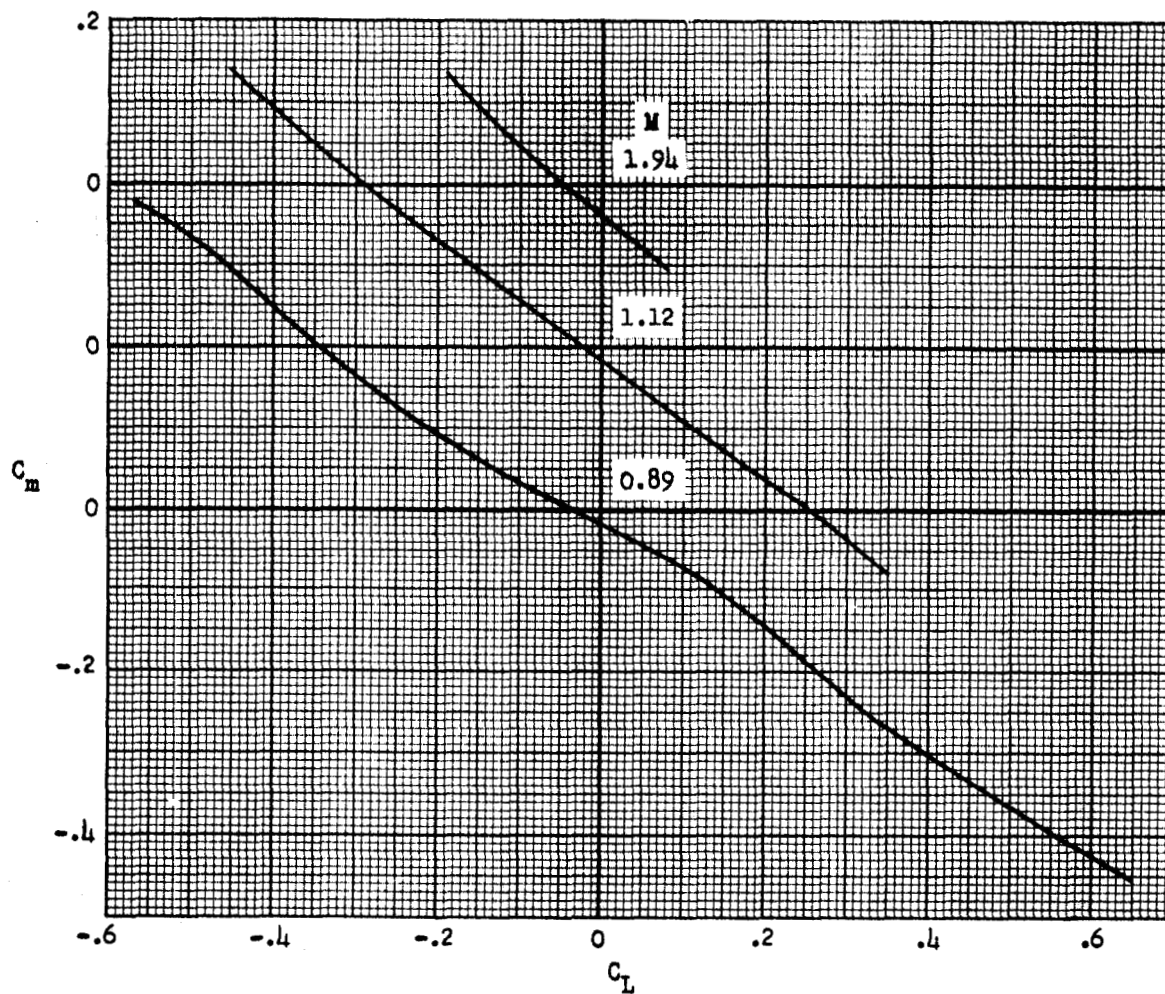
(d) Forward shift of aerodynamic center due to flexibility.

Figure 4.- Concluded.



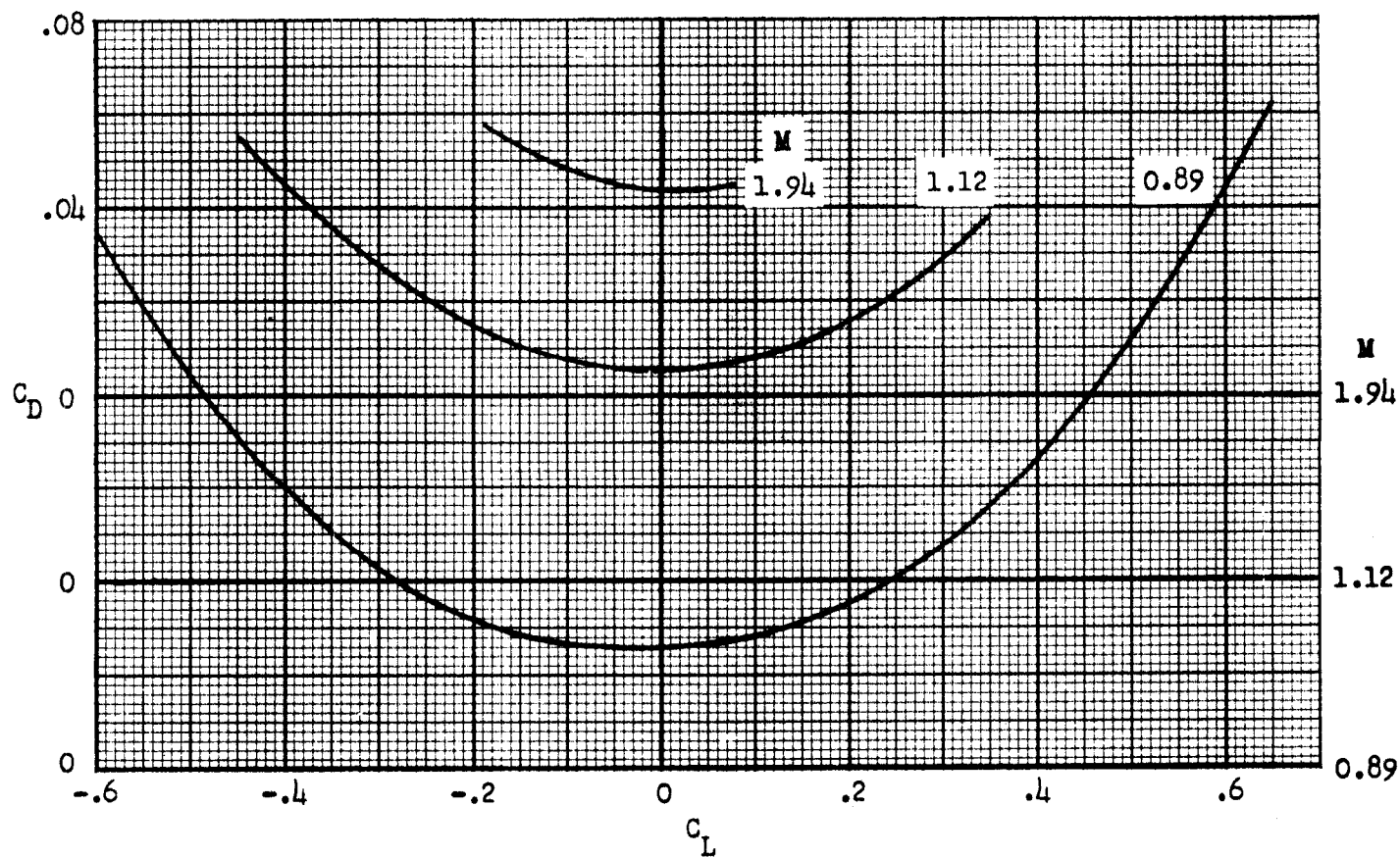
(a) Lift.

Figure 5.- Sample polars of lift, pitching-moment, drag coefficients, total pressure recovery, and mass flow.



(b) Pitching moment.

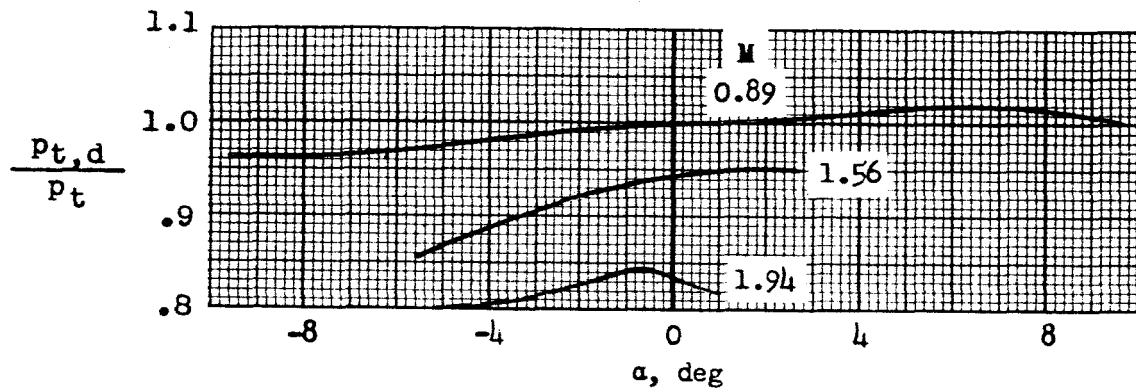
Figure 5.- Continued.



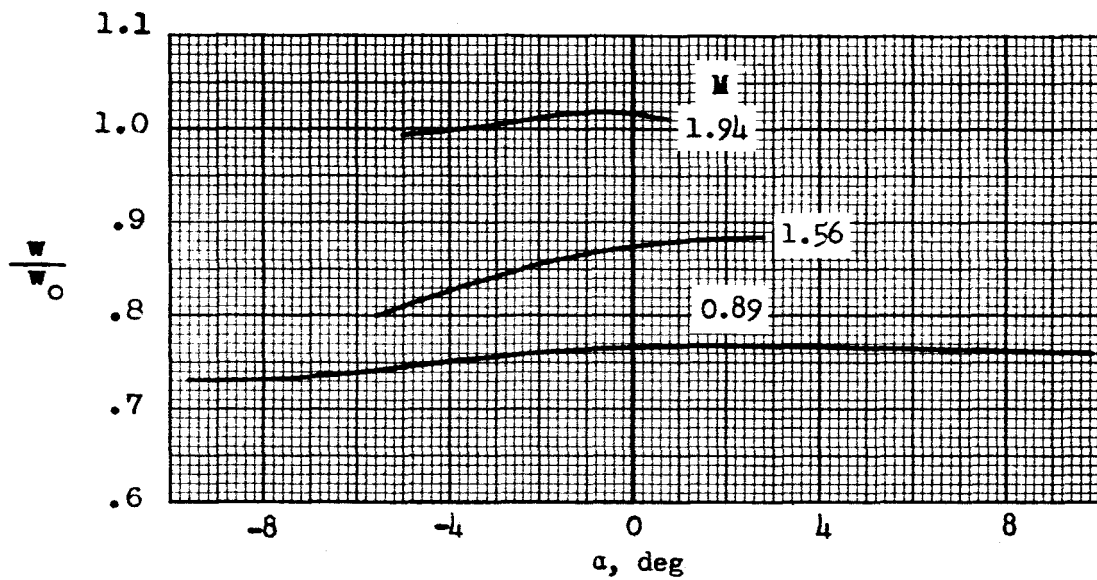
(c) Drag.

Figure 5.- Continued.

DECLASSIFIED



(d) Total pressure recovery.



(e) Mass flow ratio.

Figure 5.- Concluded.

DECLASSIFIED

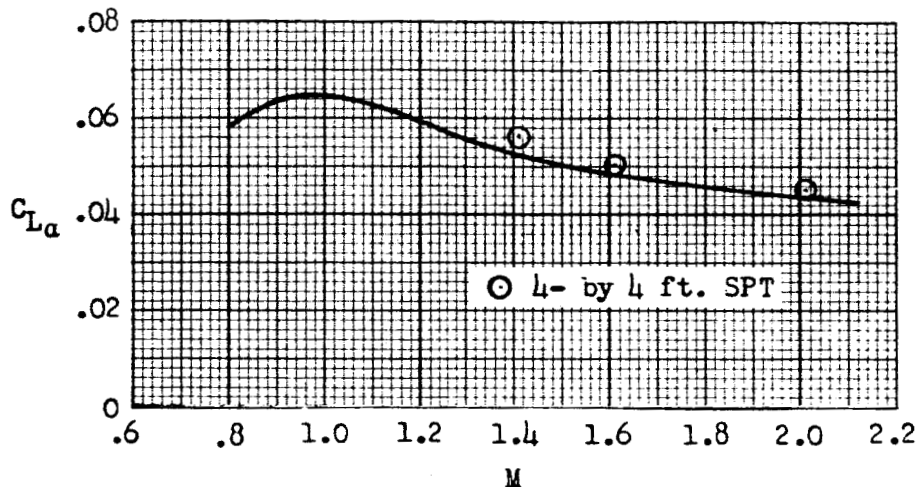
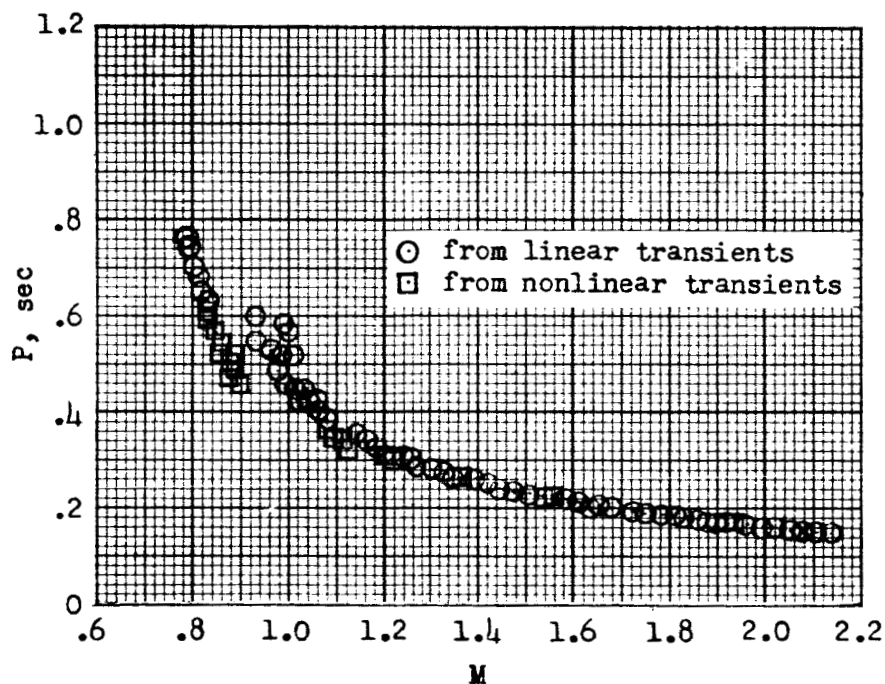


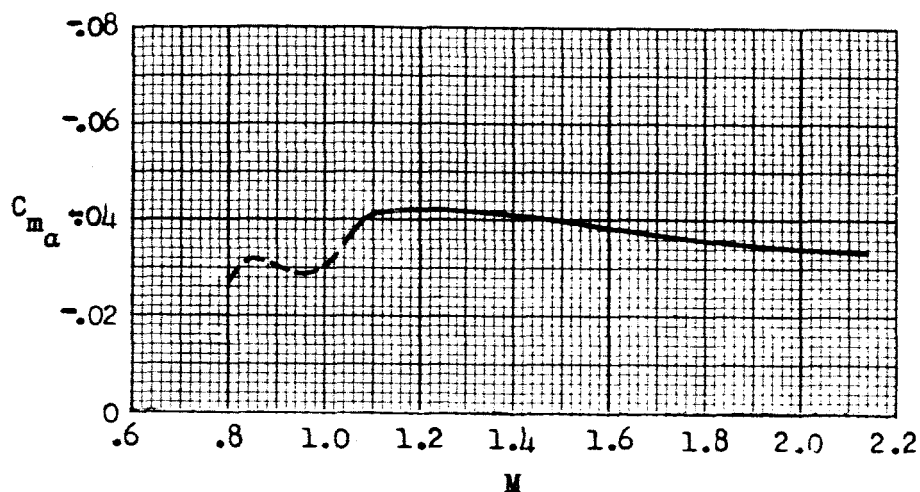
Figure 6.- Variation of lift-curve slope with Mach number.



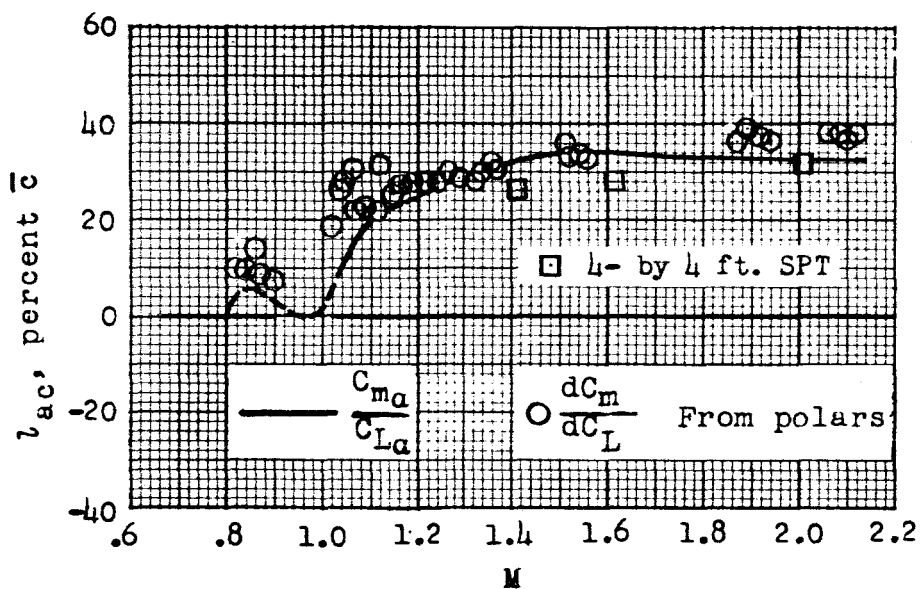
(a) Period.

Figure 7.- Variation of static longitudinal stability parameters with Mach number. Center of gravity located $0.45\bar{c}$ ahead of leading edge of \bar{c} .

DECLASSIFIED



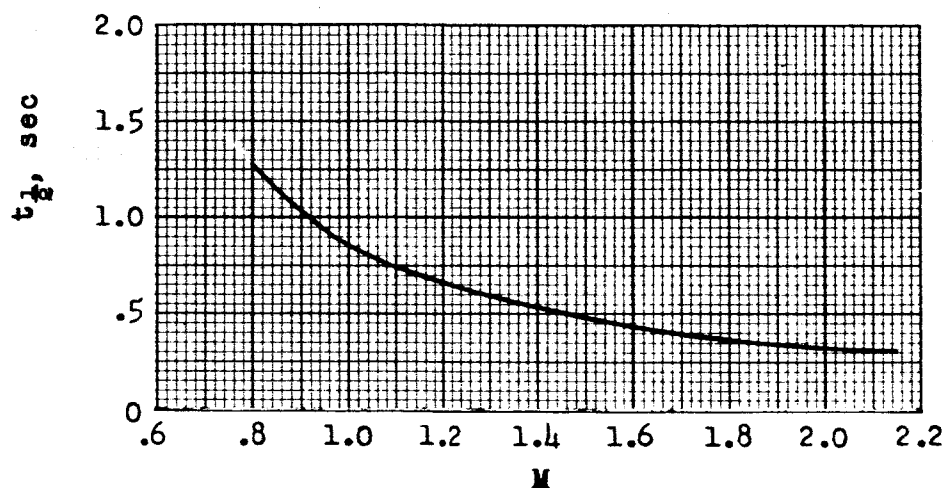
(b) Static stability derivative C_{m_α} .



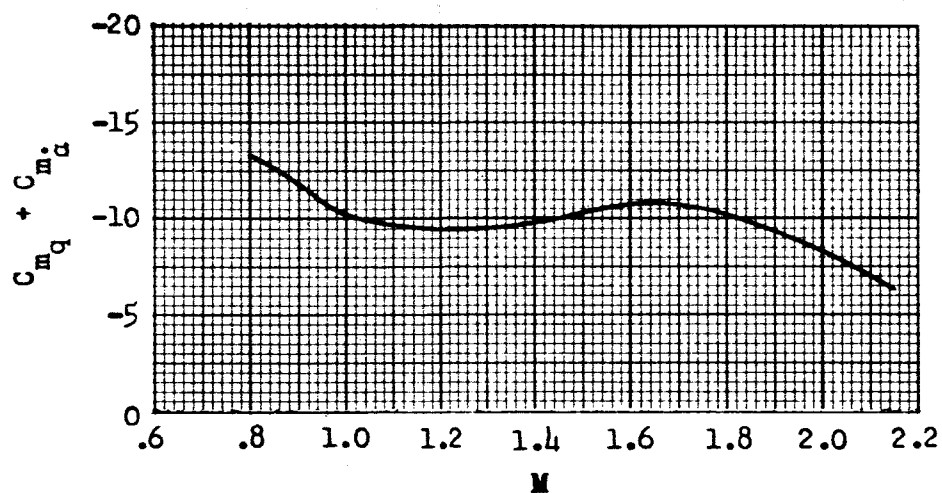
(c) Aerodynamic center.

Figure 7.- Concluded.

DECLASSIFIED



(a) Time for model to damp to one-half amplitude.



(b) Damping in pitch derivative, $(C_{mq} + C_{m\dot{\alpha}})$.

Figure 8.- Variation of damping parameters with Mach number.

DECLASSIFIED

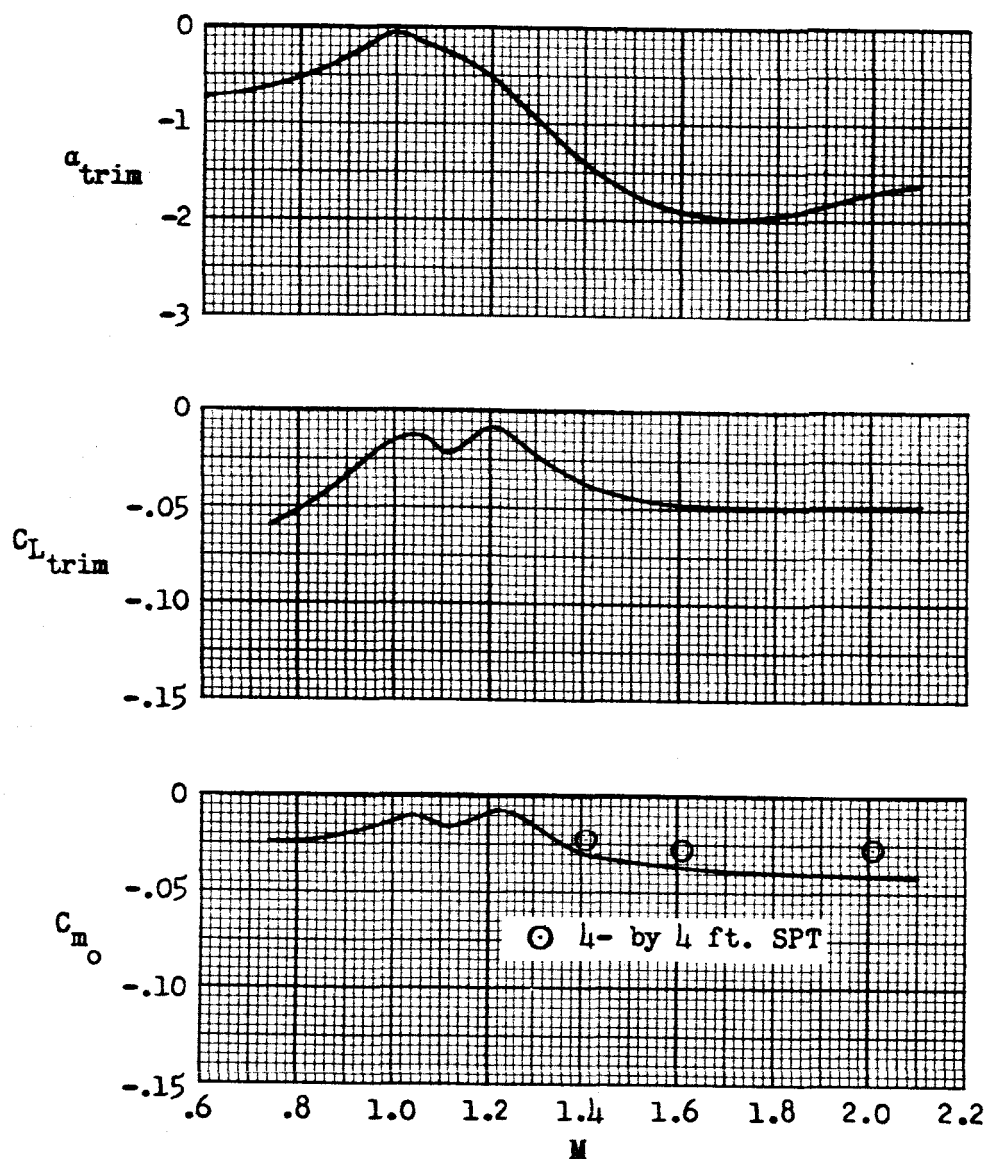
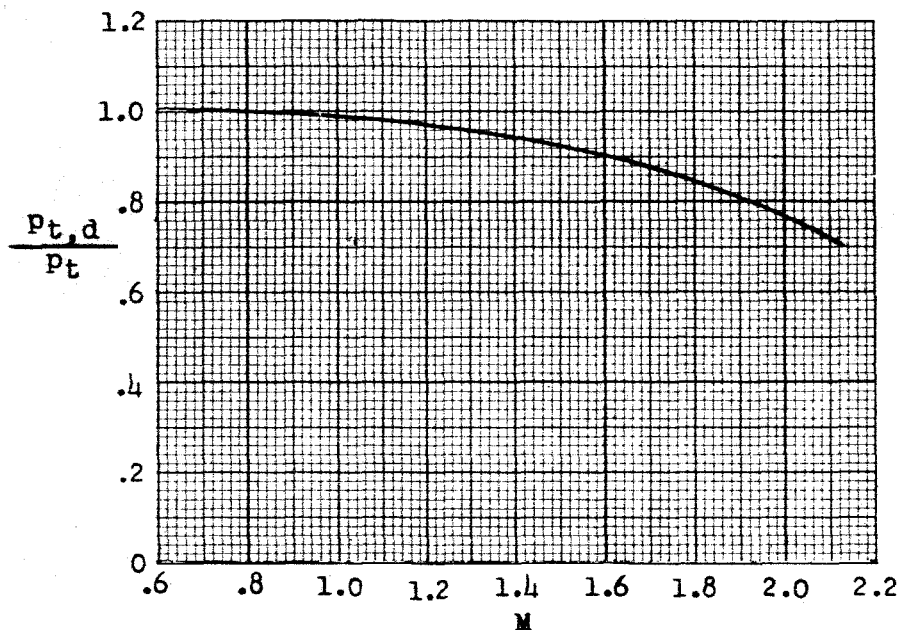
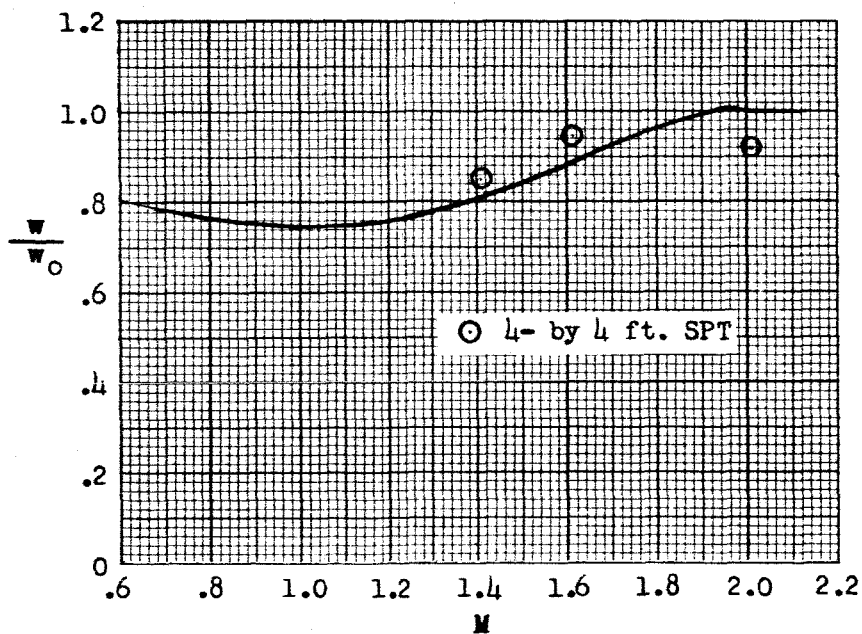


Figure 9.- Variation of trim characteristics and pitching moment coefficient at zero lift with Mach number. Center of gravity located 0.45 \bar{c} ahead of leading edge of \bar{c} .

DECLASSIFIED



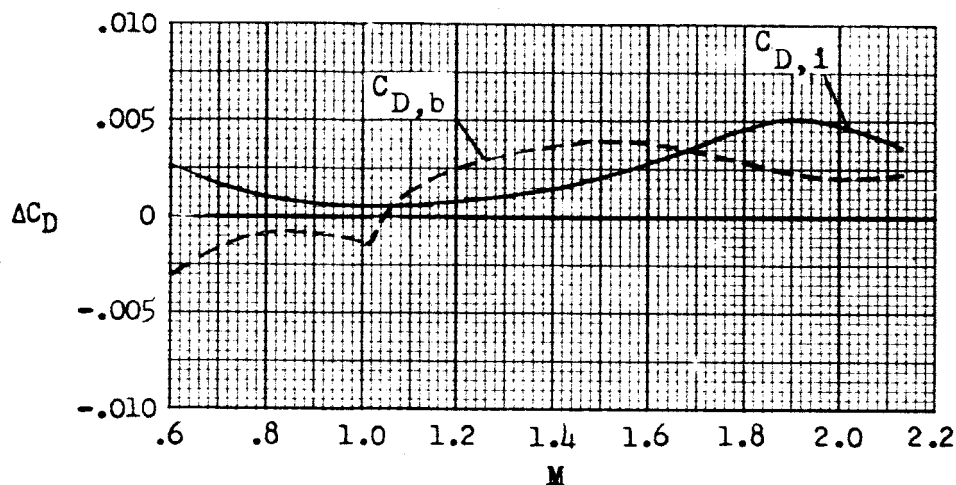
(a) Total pressure recovery.



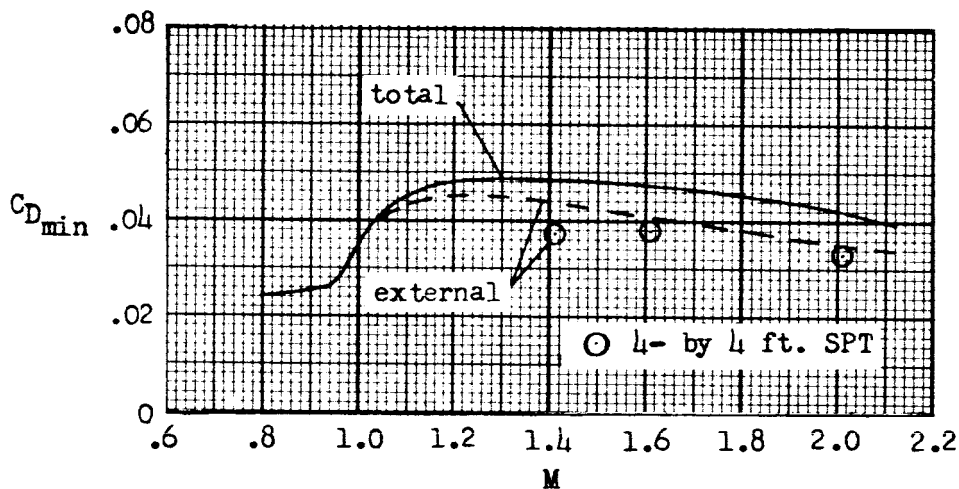
(b) Mass flow ratio.

Figure 10.- Characteristics of duct with Mach number.

DECLASSIFIED



(a) Internal and base drag. $C_L \approx 0$.



(b) Total and external drag.

Figure 11.- Variation of minimum drag characteristics with Mach number.

DECLASSIFIED

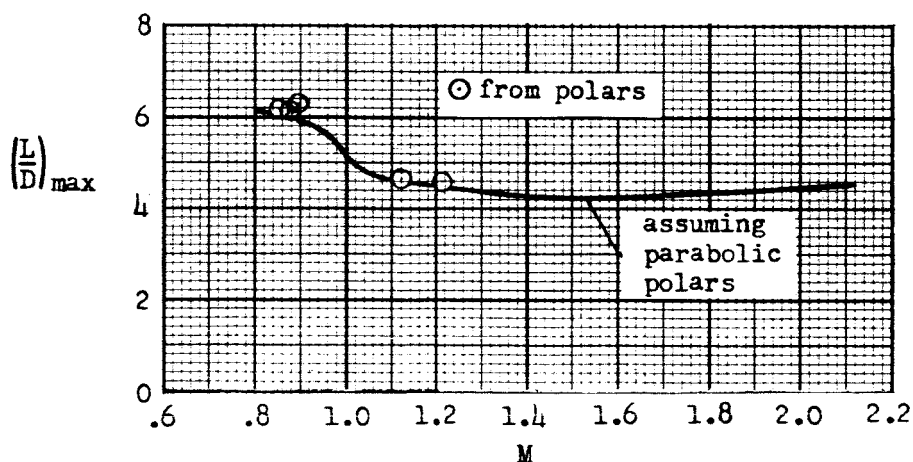
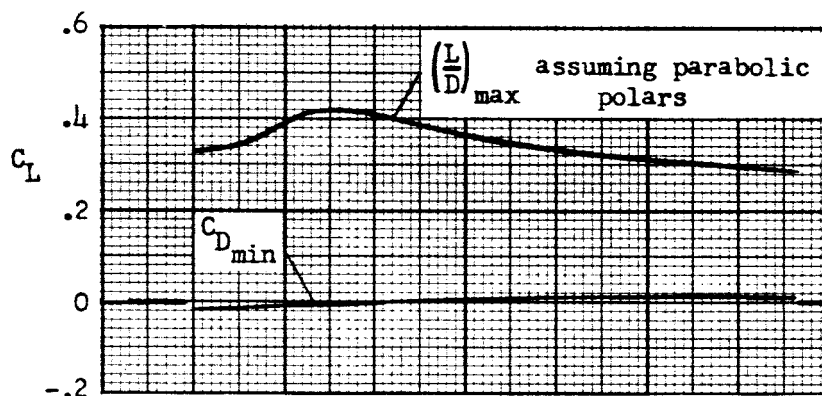
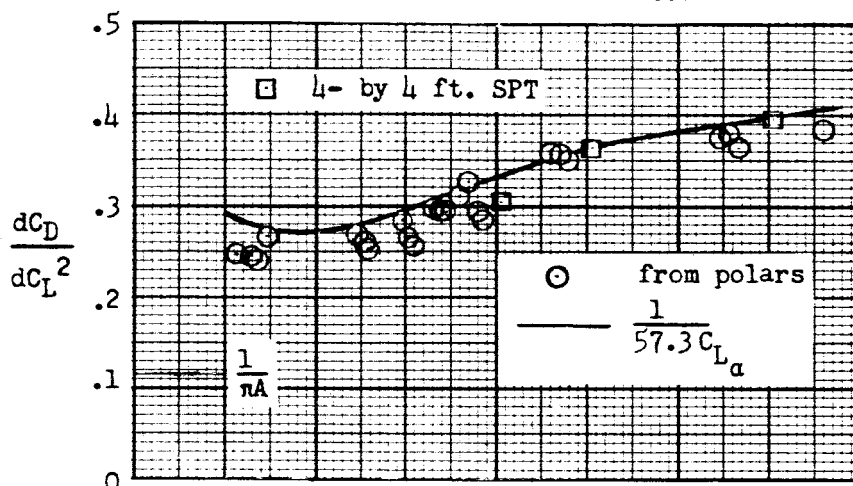


Figure 12.- Lift-drag relations for zero control deflections.



DECLASSIFIED

INDEX

<u>Subject</u>	<u>Number</u>
Bodies, Ducted	1.3.4
Air Inlets, Scoops	1.4.1.4.2
Diffusers, Supersonic	1.4.2.1.2
Missiles, Specific Types	1.7.2.2
Stability, Longitudinal - Static	1.8.1.1.1
Stability, Longitudinal - Dynamic	1.8.1.2.1
Damping Derivatives - Stability	1.8.1.2.3

ABSTRACT

The longitudinal stability and limited duct performance of the Chance-Vought Regulus II missile was determined from $M = 0.8$ to $M = 2.1$ utilizing a free-flight, 0.12-scale rocket-powered model. Data were in agreement with data from other tests and indicated that large negative pitching moments at zero lift were experienced at supersonic speeds. The underslung scoop-type duct also influenced the static stability at transonic speeds.



A 10x10 grid of 100 small squares, each containing a number from 1 to 100 in a random order.

[REDACTED]